Pergamon

Carbon Vol. 36, Nos. 1–2, pp. 1–9, 1998

0008-6223/97 $17.00

PII: S0008-6223(97)00144-9

MECHANICAL PROPERTIES OF NANOTUBULE FIBERS AND COMPOSITES DETERMINED FROM THEORETICAL CALCULATIONS AND SIMULATIONS

S. B. SINNOTT,[a,*] O. A. SHENDEROVA,[b] C. T. WHITE[c] and D. W. BRENNER[b]
[a]University of Kentucky, Department of Chemical and Materials Engineering, Lexington, KY 40506-0046, U.S.A.
[b]North Carolina State University, Department of Materials Science and Engineering, Raleigh, NC 27695-7907, U.S.A.
[c]Naval Research Laboratory, Code 6179, Washington, DC 20375-5342, U.S.A.

(*Received* 6 *May* 1997; *accepted in revised form* 1 *July* 1997)

Abstract—Theoretical Young's moduli have been estimated for carbon fibers composed of single-walled fullerene nanotubules aligned in the direction of the tubule axis. In the limit of infinitely long tubules, the fibers can have a Young's modulus comparable to that of diamond. Exploiting this property of nanotubule fibers, we investigate a new carbon composite composed of layered nanotubule fibers and diamond. Such a composite is found to be a high-modulus, low-density material that is quite stable to shear and other distortions. © 1997 Elsevier Science Ltd

Key Words—A. Nanotubes, A. carbon composites, A. diamond, C. molecular simulation, D. mechanical properties.

1. INTRODUCTION

The last two decades have witnessed phenomenal growth in the area of materials science, as a variety of new intriguing materials have been discovered and synthesized. One of the most revolutionary has been the class of carbon compounds referred to as fullerene nanotubules. Since their discovery by Iijima in 1991 [1], there has been a flurry of activity in the research community to explore their unique properties and possible applications [2].

Carbon nanotubules can be thought of as rolled up sheets of graphite that are sometimes capped on each end, with structures that vary depending on the conditions under which they are synthesized. They can be single-walled [3,4] (a single tubule) with diameters as small as about 1 nm, or multiwalled [1,5] (2 to 50 tubules positioned one within the other) with outer diameters ranging from about 5 to 350 nm. They can also have many different helical structures, and changes in the radii and helical structures have been predicted to affect the nanotubule's conducting properties, which can vary from metallic to semiconducting [6–8]. As a consequence, much work has been done to determine the electronic structure of nanotubules [9,10] and they are finding use in the formation and encapsulation of nanowires [11,12]. Nanotubules are further predicted to be highly polarizable "molecular straws" [13] that might find future applications as nanometer-scale test-tubes.

There have also been several theoretical studies of individual nanotubule elastic properties [14–18], and structure [14,17,18] that suggest that they have anomalous moduli and might be quite stiff in the direction of the tubule axis. These predictions agree with experimental observations [19] and were recently confirmed through direct measurements of the amplitude of thermal vibrations of several individual multiwalled nanotubules with a transmission electron microscope, which found an average Young's modulus in the direction of the tubule axis of 1.8 TPa [20]. The goal of the present work is to study the mechanical properties of fibers of ordered carbon nanotubules and a hypothetical structural composite which includes nanotubule fibers that, if it could be synthesized, would be an ultra-light, ultra-strong material. The mechanical properties are investigated using analytical calculations and atomistic simulations.

2. PROPERTIES OF TUBULE-BASED CARBON FIBERS

Carbon nanotubules have some properties in common with regular graphite, one of which is high stiffness in the direction of the tubule axis [14–20] which is analogous to the high stiffness within the graphite planes. However, in the direction normal to the tubule axis or graphite plane, nanotubules and graphite are soft [17,19]. Therefore, exploitation of the strength of nanotubules in applications will require an ordered, close-packed arrangement of tubules in the direction of the tubule axis.

We start by considering a pure fiber composed of single-walled nanotubules that are arranged in such a manner. To simplify the analysis, all the tubules are assumed to be identical in each fiber, and the fiber itself is assumed to be infinitely thick. The

*Corresponding author.

Young's modulus of the fiber is therefore:

$$Y_{\text{axis}} = \frac{\partial^2 E}{\partial \epsilon^2} \times A \times L \tag{1}$$

where $\partial^2 E/\partial \epsilon^2$ is the second derivative of energy with respect to strain along the tubule axis, L is the number of atoms per tubule per unit length and A is the number of tubules per unit area perpendicular to the fiber axis, which depends on the tubule radius and the closest distance between the nanotubule walls.

To further simplify the analysis we assume that the tubule diameters vary in a nondiscrete manner and the tubules themselves are of the achiral variety and therefore have either the serpentine or sawtooth structure (see ref. [16] for the definition of these structures). In addition, it is assumed that the tubules are cylindrical which, based on recent theoretical studies [14] and experimental observations [2,17] is an excellent assumption for tubules with diameters less than 4 nm. Incorporating these assumptions into eqn (1) gives the following expression for the Young's modulus:

$$Y_{\text{axis}} = \frac{\partial^2 E}{\partial \epsilon^2} \times \frac{0.9 \times 4 D_t}{3\sqrt{3} d^2 \left(0.5 D_t + \dfrac{R_{\text{vdW}}}{2}\right)^2} \tag{2}$$

where D_t is the tubule diameter, R_{vdW} is the closest distance between walls, 0.9 is the packing fraction for a two-dimensional hexagonal lattice and d is the bond length.

Figure 1 shows how the Young's modulus from eqn (2) varies with the inter-tubule distance R_{vdW} for fibers of various diameters (solid lines). Also shown as dashed lines are moduli for diamond in the (111) direction as well as ideal graphite, a graphite whisker and a silicon nitride whisker, thus allowing for direct comparisons between the nanotubule fibers under study and these traditional fibers. The figure shows several important trends. The first is that macroscopic fibers composed of close-packed tubules that are 0.315 nm apart with diameters of 1.0 nm (size and distance ranges which have been experimentally observed [1,21]), have a modulus that is close to that of a traditional graphite whisker, around 0.77 TPa. As the radius of the tubules decreases, the Young's modulus increases, a trend that is also observed experimentally for multiwalled tubules [20].

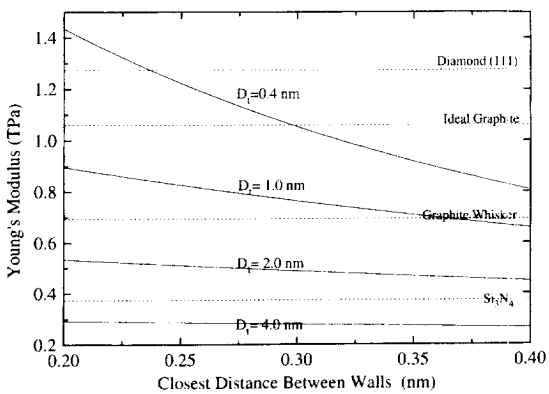

Fig. 1. The solid lines are the Young's moduli of a nanotube fiber using eqn (1) as a function of the tubule radii and the closest distance between the tubule walls. The dashed lines are the Young's moduli of well-known high modulus materials shown for comparison.

Figure 1 also shows that fibers composed of smaller radius carbon nanotubules packed about 0.1 nm closer together have moduli around 1.25–1.40 TPa, which is greater than the modulus of either in-plane graphite or diamond (111). It should be noted, however, that these curves were generated assuming infinitely long tubules with an in-plane graphite value of 58.2 eV atom^{-1} for $\partial^2 E/\partial \epsilon^2$ independent of tubule diameter (calculated as c_{11} for graphite divided by its density [16]). This is a reasonable upper bound as previous studies [16] have shown that tubules get only slightly softer as their diameters decrease in the range of diameters shown in Fig. 1 [22].

The calculated Young's moduli for the macroscopic tubule fibers show fair agreement with measured and calculated single-tubule moduli. For example, the direct experimental measurements of the moduli of single, multiwalled tubules [20] gave an average value of 1.8 TPa. The tubule with the smallest inner diameter was considerably stiffer, with a modulus of 3.70 TPa. Theoretical estimates of the modulus of single-walled nanotubules range from 5.5 TPa (determined from the data in ref. [16] and assuming a tubule wall thickness of 0.066 nm) [18], to 5.2 TPa (estimated from bending rigidity calculations) [15], to 1.4 TPa (determined from tight-binding calculations) [17]. Very recently, the Young's moduli of a series of single-walled tubules were determined using the reactive-empirical bond-order hydrocarbon potential discussed in detail below and were found to range from 1.5 TPa at diameters of about 0.5 nm to 0.3 TPa at diameters of about 5.0 nm [23].

A previous theoretical study using similar analytical arguments [24] indicates that while multiwalled tubules also show improved mechanical properties when placed in a close-packed arrangement, the improvement is not as significant as for the single-walled tubules.

3. PROPERTIES OF DIAMOND–TUBULE FIBER COMPOSITE STRUCTURES

The data presented above confirms previous predictions that fibers composed of multiple, close-packed carbon nanotubules are promising high-modulus materials. It is not clear, though, how such fibers could be stabilized against shear, where the tubules would slide by one another with little resistance. We therefore examine a hypothetical composite material that, if it could be produced, would exploit the nanotubule fiber's high modulus and light weight,

and at the same time stabilize the material against shear.

The composite material consists of covalently bonded layers of diamond and close-packed, nanotubule fibers. Diamond was chosen as it is a high-modulus material which can form strong covalent chemical bonds with the tubule fiber. On the diamond (111) surface, each carbon atom has six carbon neighbors which form a hexagonal arrangement at a distance equal to the second neighbor position in bulk diamond of 0.252 nm. These surface carbon atoms can bond to an open (not capped) sawtooth tubule of type (6,0) (with a diameter of 0.476 nm) aligned normal to the surface with a mismatch in diameter of about 5%. The sp^3 radical orbitals associated with the carbon atoms on the diamond (111) surface are directed normal to the surface and would therefore overlap strongly with those at the end of the sawtooth tubule leading to strong covalent bonds between the two materials. Therefore, adhesion between the nanotubule fiber and diamond layers would be accomplished through covalent bonding eliminating the need for adhesives and special heating treatments [25].

An example of the resulting composite is shown in Fig. 2 where the tubule packing in the plane of the diamond surface is 38.46 $Å^2$ $tubule^{-1}$ (the carbon atoms on the diamond (111) surface that are not bonded to the end of a carbon nanotubule are hydrogen-terminated to satisfy the atoms' valence requirements). The composite structure not only keeps the tubules from sliding past one another, thus stabilizing the nanotubule fiber against shear, it also forces the tubules to be about 0.2 nm apart, which according to Fig. 1 is the region where the fiber has its highest modulus. Compression of the nanotubule fiber will therefore be necessary to obtain the composite structure which will be strained and therefore prone to defects.

Recently, electron beam evaporation has been used to create multilayer, close-packed nanotubule films (the tubules were 4–20 nm in diameter) on silicon (111) surfaces [26]. While there are significant differences between the experimental tubule–silicon interface and the theoretical tubule–diamond interface shown in Fig. 2 [27], this study shows that layers of close-packed tubules can be formed on the (111) surface of diamond-structured materials. Fine-tuning the growth conditions to favor smaller diameter, single-walled, open-ended nanotubules [2] and a freshly sputtered (111) silicon surface would bring the experimental interface structure even closer to the proposed composite interface structure. Because of the larger lattice constant in silicon, compression of the tubule fiber will not be necessary to achieve the covalent bonding between the tubules and the silicon.

According to eqn (2), the fiber portion of the composite would have a Young's modulus of 1.32 TPa in the limit of infinitely long tubules. The Young's modulus of diamond (111) can be calculated

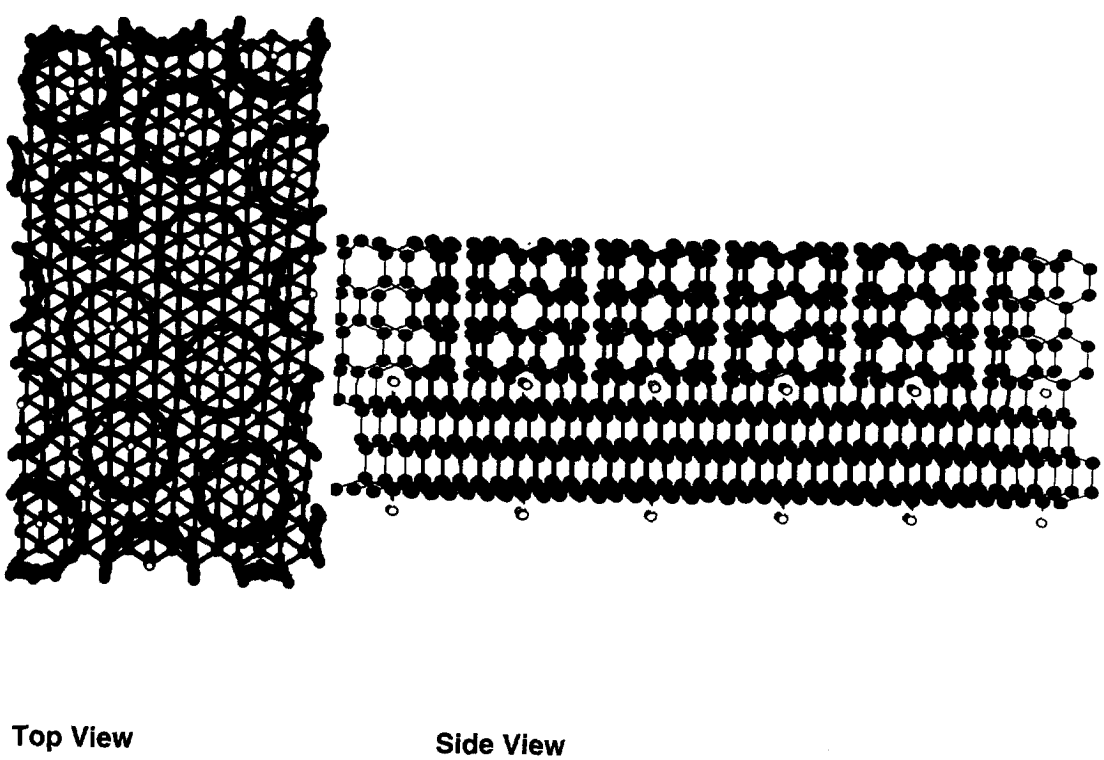

Fig. 2. The tubule–diamond carbon composite unit cell. The gray atoms are carbon and the white atoms are hydrogen. The sawtooth tubules are of the (6,0) type and each has a diameter of 0.476 nm.

from the experimental elastic constants c_{ij} using [28]

$$Y_{\text{diamond (111)}} = \frac{6c_{44}(c_{11}+2c_{12})}{c_{11}+2c_{12}+4c_{44}} \quad (3)$$

and is found to be 1.27 TPa. Thus, the Young's modulus of an infinitely long fiber composed of tubules of the size and arrangement of the composite is predicted to have a Young's modulus in the direction of the tubule axis that exceeds the Young's modulus of diamond in the (111) direction by 4% at a density that is about 80% of the density of diamond.

To determine how the modulus of the composite structure changes when it is composed of diamond layers of different thicknesses and fibers of varying finite tubule lengths, several composites were subjected to tensile strain and the resulting stresses calculated using the reactive-empirical bond-order potential for hydrocarbons developed by Brenner [29] (see Appendix A for potential details). The potential yields elastic constants for diamond of $c_{11}=10.78\times10^{11}$ N m^{-2}, $c_{12}=1.31\times10^{11}$ N m^{-2} and $c_{44}=6.8\times10^{11}$ N m^{-2}, which are in good agreement with the experimental values of $c_{11}=10.76\times10^{11}$ N m^{-2}, $c_{12}=1.25\times10^{11}$ N m^{-2} and $c_{44}=5.8\times10^{11}$ N m^{-2} [30]. These elastic constants give a value for Y_{diamond} of 1.35 TPa, which is 6.3% higher than the experimental value. The potential is fit to, and therefore reproduces exactly, the in-plane modulus of graphite.

The Young's modulus of the composite discussed above (same tubule type and diameter) as a function of tubule length (thickness of the fiber layer) and diamond layer thickness is shown in Fig. 3. For a given tubule length, as the thickness of the diamond layer increases, the modulus of the composite increases. In addition, as the fiber layer thickness increases, or the tubules increase in length, the Young's modulus of the composite increases such that the curves appear to be converging to a value of about 1.34 TPa, which is very close to the value that the potential gives for pure diamond in the (111) direction. An advantage of the short nanotubules for these high strength composites is that they maximize the tubule–diamond covalent interactions which occur only at the ends of the tubules. As the fiber dominates the composite structure at long tubule lengths, however, the overall density of the composite decreases significantly, as shown in Fig. 4. Thus, the calculations predict that the proposed fiber–diamond composites can have a Young's modulus that is approximately the same as diamond in the (111) direction at densities that are 86–97% that of pure diamond.

Part of the motivation for building the composite is to use the diamond layers to stabilize the tubule fiber against shear and other distortions [15,16]. To check how well the diamond stabilizes the fiber and investigate the stability of the strained tubule–diamond covalent bonds, we performed two sets of molecular dynamics simulations with the reactive-empirical bond-order potential in which tensile and shear strains were applied to the composite shown in Fig. 2 and discussed above. In these simulations the tubules were approximately 0.8 nm long, while the diamond layers were approximately 0.5 nm thick in the tension-loading simulations and 1.0 nm thick in the shear-strain simulations, which corresponds to 1260 carbons atoms and 28 hydrogen atoms, and 3024 carbon atoms and 28 hydrogen atoms, respectively. Periodic boundary conditions were applied in three dimensions for the tension-loading simulations, while a combination of periodic boundary conditions in the plane of the tubule fiber–diamond contact and rigid boundary conditions in the outer diamond planes perpendicular to the fiber axis were used in the shear-strain simulations. In each case a time step of 0.5 femtoseconds was used and the deformation rate was 1% per 100 femtoseconds. This deformation rate is comparable to those following penetration of the composite by a projectile [31].

Atomic level stress evolution in the composite was

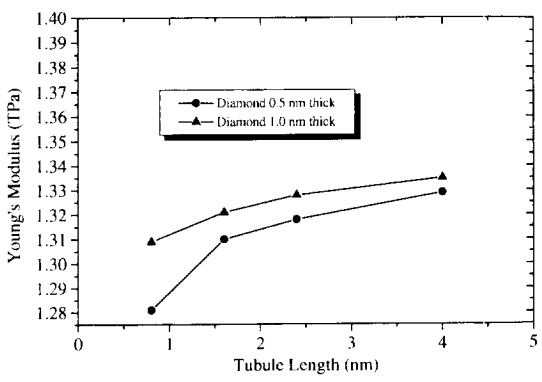

Fig. 3. The Young's moduli of the tubule–diamond composite shown in Fig. 2 as a function of tubule length and diamond thickness as determined from calculations with the reactive-empirical bond-order potential.

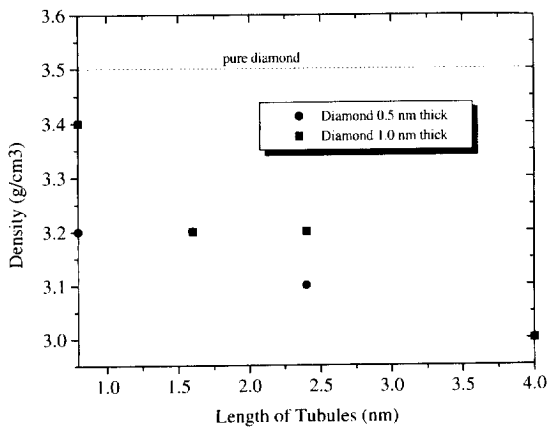

Fig. 4. The density of the tubule–diamond composite shown in Fig. 2 as a function of tubule length and diamond thickness.

monitored during deformation. The observed atomic stresses attributed to individual atoms are the sum of the moments of forces exerted by neighboring atoms on each atom per atomic volume [32]. The invariant stress characteristics were calculated including the local hydrostatic stress, which describes the local density fluctuations, and the von'Mises shear stress, which is the mean square of the shear stress averaged over all orientations in the solid [33]. The later stress invariant describes the distortion of the local topology of each atom.

In the first set of molecular dynamics simulations, a tensile strain was applied in the direction of the fiber axis as shown in Fig. 5. The distribution of the hydrostatic stresses within the composite during deformation is indicated in the snapshots by color-coding the carbon atoms. Figure 5(a) shows that there are small stresses at the tubule–diamond interface before loading. The atoms in the diamond layers closest to the tubule fiber (atoms D in Fig. 5(a)) are under slight tension while the atoms at the ends of the tubules (atoms T in Fig. 5(a)) are under slight compression. This intermediate layer of atoms at the ends of the tubules have one sp^3-hybridized neighbor (with a bond length of 1.52 Å) and two sp^2-hybridized neighbors (with bond lengths of 1.42 Å) and therefore have some radical character associated with them. The strained atoms at the fiber–diamond interface (D and T atoms in Fig. 5) explain why the composite's Young's modulus is smaller than the modulus of either diamond or the infinitely long tubule fiber when thin layers of diamond and fiber are used (see Fig. 3). As the thickness of the fiber and diamond layers increases, the modulus of the composite increases because the strained interface atoms make up a smaller fraction of composite atoms.

The stress distributions at the tubule fiber–diamond boundary are similar to the stresses arising on free diamond (111) surfaces, where the first surface layer of atoms have only one neighbor; these atoms are therefore identical to those on the ends of the tubules. The stresses at the tubule–diamond boundary can also be thought of as originating from the mismatch between graphite bond lengths and the $\langle 111 \rangle$ projection of the diamond bond lengths (which are about 2% longer). This mismatch puts the diamond atoms which are not fully saturated under compression and puts their nearest neighbors in the tubules under slight tension (0.7%, which is not seen at the figure on the given stress scale).

After the tensile forces are applied, the tubules stretch elastically to about 24% of their equilibrium length. Additional tensile forces cause the composite

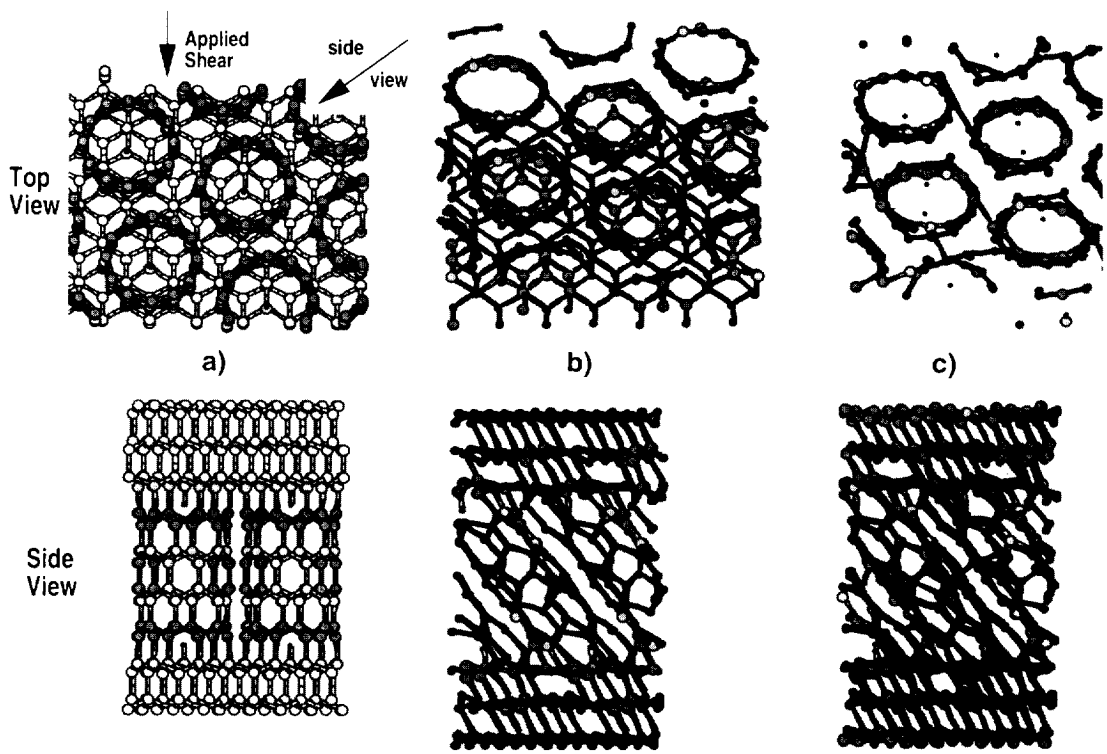

Fig. 5. Snapshots from molecular dynamics simulations using the reactive-empirical bond-order potential of the composite shown in Fig. 2 under applied tension. The small spheres represent hydrogen atoms and the larger spheres represent carbon atoms. The carbon atoms are color-coded according to the local hydrostatic stresses (in eV $Å^{-3}$) – slate gray: $-0.05 \sim -0.01$; white: $-0.01 \sim 0.01$; light gray: $0.01 \sim 0.4$; black: above 0.4. (a) strain $= \epsilon = 0$, (b) $\epsilon = 24\%$, (c) $\epsilon = 24.5\%$ ($T = 0$ K), (d) $\epsilon = 32\%$ ($T = 300$ K).

to fail and the failure mechanism depends to a large degree on the system temperature. Due to a Poisson ratio of 0.5 at high deformation, the tubules compress perpendicular to their axis during stretching (see Fig. 5(b)). This causes the distances between the atoms in the narrowest part of each tubule to decrease to such a large degree that second-neighbor atoms near the vertex of the six-atom rings interact with each other. It therefore becomes favorable for the system to form a structure with five-atom rings in the narrowest parts of the tubules, which destroys the integrity of the tubule structure and leads to failure of the composite (see Fig. 5(c)). The energy per atom of the resulting cupped structure is equal to the energy per atom of the composite stretched by about 16%. Hence, at zero temperature, the rebonding mechanism of failure dominates. In contrast, at room temperature rebonding also occurs but at different times for different tubule atoms, thus causing the new bonds to spread in arbitrary directions (see Fig. 5(d)). The end result is therefore a mass of networked carbon–carbon chains where the tubules use to be, with the diamond substrate remaining nearly perfectly ordered. The final separation of the composite in this case occurs when the composite has been deformed by about 35%. These values of maximum tubule strain before failure show good agreement with values determined for a single carbon nanotubule using the same potential [18].

In the second set of simulations, a shearing strain was applied along the direction close to one of the three directions where the tubules are most densely packed. The snapshots of the von'Mises shear stress distribution at different shear strains are shown in Fig. 6. Figure 6(a) shows that prior to shearing, the composite contains some residual shear stresses within the tubules and the first layer of the diamond. As the shear forces are applied, it is clear that the maximum shear stress for both the diamond and the tubule fiber is concentrated near the tubule–diamond boundary where the tubules connect to the diamond at an obtuse angle (Fig. 6(b)). The maximum hydrostatic tension in the system is also located in this area.

Atoms with broken bonds in the diamond layers near this region of maximum shear stress can be seen in the bottom of Fig. 6(b). On the other hand, minimum shear stresses (and hydrostatic compression) are observed near the tubule–diamond boundary where the fiber and diamond form an acute angle (the gray atoms in Fig. 6(b)). The minimum shear stresses within the diamond are situated along the extension of the tubules axis into the diamond (the gray atoms can be seen inside the tubule openings at the top of Fig. 6(b)).

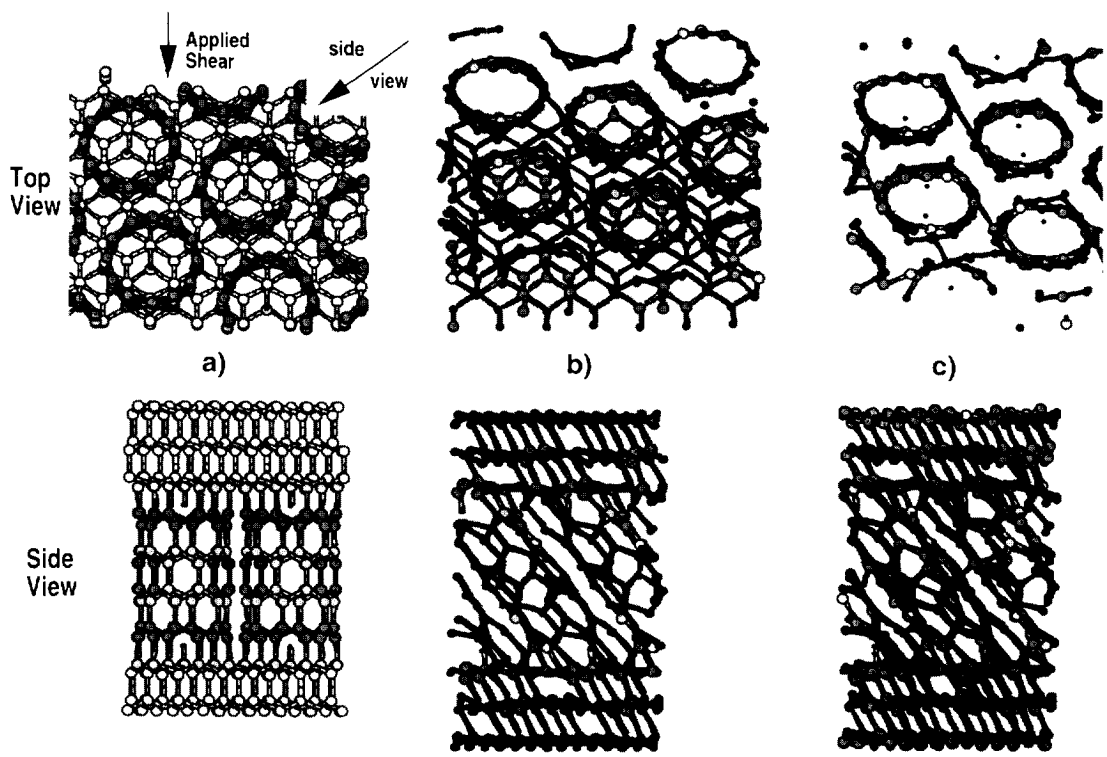

Fig. 6. Snapshots from molecular dynamics simulations using the reactive-empirical bond-order potential of the composite shown in Fig. 2 under applied shear. The small spheres represent hydrogen atoms and the larger spheres represent carbon atoms. The carbon atoms are color-coded according to the local von'Mises stresses (in eV Å^{-3}) – white: 0.~0.1; light gray: 0.1~0.3; slate gray: 0.3~0.6; black: above 0.6. (a) shear strain $=\gamma=0$, (b) $\gamma=0.45$ ($T=0$ K), (c) $\gamma=0.45$ ($T=300$ K).

As the shear forces continue to be applied, the initially perfectly cylindrical tubules became oval in the projection along the tubule axis (Fig. 6(b) and (c), top pictures). Consequently, the distance between the tubules decreases and at a shear strain of 0.4, covalent bonds are formed between the tubules (Fig. 6(c)). At room temperature there are many more links between the tubules (Fig. 6(c)) then in the composite at zero temperature at the same strain point (Fig. 6(b)). At even higher shear loads, the disordering within the tubules increases until the composite turns into layers of diamond separated by layers of amorphous carbon.

The observed disorder of the carbon nanotubules following deformation of the composite is comparable to the results of simulations [15,34], where single nanotubules are subjected to compressive, twist and shear strains of approximately 15–25%. In the composite, tubule disorder seems to be preferred over delamination (a common problem in structural composites [25]) at the deformation rates under study here. This disorder of the tubules therefore represents a mechanism by which the composite could absorb and dissipate energy from a projectile.

4. SUMMARY

The theoretical Young's modulus has been calculated for several carbon fibers composed of fullerene nanotubules aligned in the direction of the tubule axis. The results show that fibers composed entirely of single-walled tubules have a high modulus which increases as the tubule radii decrease and as the distance between the close-packed tubules in the fiber gets shorter. We also propose a new, strongly bonded, high modulus, low density, tubule fiber–diamond structural composite that is relatively stable to shear and tensile distortions at rates corresponding to high-speed projectile impacts.

Acknowledgements—Some of the molecular dynamics simulations were performed on the NASA-Ames High Performance Computing and Communications Program (HPCCP)/Computational Aerosciences (CAS) Parallel Systems through a grant of computer time from NASA-Ames to S. B. S. This work was also partially supported by the Office of Naval Research through the Naval Research Laboratory (# N00014-94-WX-23024), the University of Kentucky (# N00014-95-1-1183) and North Carolina State University (# N00014-95-1-0270). Finally, S. B. S. and D. W. B. gratefully acknowledge an Oak Ridge Associated Universities Junior Faculty Enhancement Award and a National Science Foundation CAREER development grant, respectively.

APPENDIX A

The reactive-empirical bond-order (REBO) potential is short-ranged and accurately describes the covalent bonding in small organic molecules, including radicals, in addition to diamond and graphite surfaces. The potential has already been successfully applied to many interesting materials science problems such as the sputtering [35], compression [36], indentation [37], reaction [38], friction [39] and patterning [40] of diamond surfaces, the formation of fullerenes from graphitic ribbons [41], and the reaction of a surface molecule with a gas-phase molecule [42]. To model the cohesive van der Waals interactions that exist between the nanotubules, a long-range Lennard–Jones potential is added that becomes activated only after the short-ranged REBO potential goes to zero.

The combined expression for the binding energy is:

$$\text{Binding Energy} = \sum_i \sum_{i>j} [V_R(r_{ij}) - B_{ij} V_A(r_{ij}) + V_{vdW}(r_{ij})] \quad (4)$$

where V_R is a pair-additive term that takes into account the interatomic repulsive interactions (core–core), V_A is a pair-additive attractive energy arising from interactions between the valence electrons and the cores, r_{ij} is the distance between atoms i and j, and B_{ij} is a many-body empirical bond-order term. V_{vdw} is the van der Waals energy and is evaluated as follows:

$$V_{vdw} = \begin{cases} 0.0 & r_{ij} \le r_{small} \\ \{c_{3,k}(r_{ij}-r_k)^3 + c_{2,k}(r_{ij}-r_k)^2 + c_{1,k}(r_{ij}-r_k) + c_{0,k}\} & r_{small} < r_{ij} < r_{medium} \\ \{4\epsilon[(\sigma/r_{ij})^{12} - (\sigma/r_{ij})^6]\} & r_{medium} \le r_{ij} \le r_{big} \end{cases} \quad (5)$$

The parameters used in eqn (5) for the carbon–carbon van der Waals interactions are provided in Table 1 except for the coefficients for the spline, $c_{n,k}$ which are shown in Table 2.

Table 1. The parameters used in eqn (5) for the carbon–carbon van der Waals interactions (excluding the spline coefficients)

$\epsilon^a = 4.2038 \times 10^{-3}$ eV
$\sigma^a = 0.337$ nm
$r_{small} = 0.228$ nm
$r_{medium} = 0.340$ nm
$r_{big} = 1.00$ nm

[a] Parameters from ref. [43].

Table 2. The spline coefficients used in eqn (5) for the carbon–carbon interactions

r	$c_{0,k}$	$c_{1,k}$	$c_{2,k}$	$c_{3,k}$
2.0200	0.00000	0.00000	0.00000	0.00000
2.0400	0.00000	0.00000	0.00000	0.00000
2.0600	0.00000	0.00000	0.00000	0.00000
2.0800	0.00000	0.00000	0.00000	0.00000
2.1000	0.00000	0.00000	0.00000	0.00000
2.1200	0.00000	0.00000	0.00000	0.00000
2.1400	0.00000	0.00000	0.00000	0.00000
2.1600	0.00000	0.00000	0.00000	0.00000
2.1800	0.00000	0.00000	0.00000	0.00000
2.2000	0.00000	0.00000	0.00000	0.00000
2.2200	0.00000	0.00000	0.00000	0.00000
2.2400	0.00000	0.00000	0.00000	0.00000
2.2600	0.00000	0.00000	0.00000	0.00000
2.2800	0.00000	0.00000	0.00000	0.00000
2.3000	0.00000	0.00000	0.82031×10^{-1}	-0.80651×10^{-1}
3.2400	0.54952×10^{-2}	-0.59571×10^{-1}	0.15530	−0.22500
3.2600	0.43641×10^{-2}	-0.53629×10^{-1}	0.14110	−0.20750
3.2800	0.33463×10^{-2}	-0.48234×10^{-1}	0.12905	−0.21750
3.3000	0.24315×10^{-2}	-0.43333×10^{-1}	0.11615	−0.16250
3.3200	0.16100×10^{-2}	-0.38882×10^{-1}	0.10600	−0.16500
3.3400	0.87344×10^{-3}	-0.34840×10^{-1}	0.96150×10^{-1}	−0.14500
3.3600	0.21394×10^{-3}	-0.31168×10^{-1}	0.87400×10^{-1}	−0.13500
3.3800	-0.37554×10^{-3}	-0.27834×10^{-1}	0.79325×10^{-1}	−0.12000
3.4000	-0.90145×10^{-3}	-0.24805×10^{-1}	0.71819×10^{-1}	−0.10406
3.4400	-0.17854×10^{-2}	-0.19559×10^{-1}	0.59800×10^{-1}	−0.10500
3.4600	-0.21535×10^{-2}	-0.17293×10^{-1}	0.53600×10^{-1}	-0.72500×10^{-1}
3.4800	-0.24785×10^{-2}	-0.15236×10^{-1}	0.49350×10^{-1}	-0.90000×10^{-1}
3.5000	-0.27642×10^{-2}	-0.13370×10^{-1}	0.44350×10^{-1}	-0.67500×10^{-1}
3.5200	-0.30144×10^{-2}	-0.11677×10^{-1}	0.39850×10^{-1}	-0.50000×10^{-1}
3.5400	-0.32324×10^{-2}	-0.10143×10^{-1}	0.36675×10^{-1}	-0.63750×10^{-1}
3.5600	-0.34211×10^{-2}	-0.87525×10^{-2}	0.33400×10^{-1}	-0.63750×10^{-1}
3.5800	-0.35833×10^{-2}	-0.74930×10^{-2}	0.29695×10^{-1}	-0.39750×10^{-1}
3.6000	-0.37216×10^{-2}	-0.63529×10^{-2}	0.26860×10^{-1}	-0.35750×10^{-1}
3.6200	-0.38382×10^{-2}	-0.53214×10^{-2}	0.24845×10^{-1}	-0.51250×10^{-1}
3.6400	-0.39351×10^{-2}	-0.43891×10^{-2}	0.22255×10^{-1}	-0.40000×10^{-1}
3.6600	-0.40143×10^{-2}	-0.35469×10^{-2}	0.19285×10^{-1}	-0.95000×10^{-2}
3.6800	-0.40776×10^{-2}	-0.27869×10^{-2}	0.18530×10^{-1}	-0.46750×10^{-1}
3.7000	-0.41263×10^{-2}	-0.21018×10^{-2}	0.15930×10^{-1}	-0.17000×10^{-1}
3.7200	-0.41621×10^{-2}	-0.14850×10^{-2}	0.15017×10^{-1}	-0.38325×10^{-1}
3.7400	-0.41861×10^{-2}	-0.93033×10^{-3}	0.12647×10^{-1}	-0.65250×10^{-2}
3.7600	-0.41997×10^{-2}	-0.43228×10^{-3}	0.11769×10^{-1}	-0.20258×10^{-1}
3.7800	-0.42038×10^{-2}	0.14177×10^{-4}	0.10900×10^{-1}	-0.30432×10^{-1}
3.8000	-0.41994×10^{-2}	0.41365×10^{-3}	0.93680×10^{-2}	-0.15025×10^{-1}
3.8200	-0.41875×10^{-2}	0.77034×10^{-3}	0.80610×10^{-2}	-0.39000×10^{-2}
3.8400	-0.41689×10^{-2}	0.10881×10^{-2}	0.79250×10^{-2}	-0.29000×10^{-1}
3.8600	-0.41442×10^{-2}	0.13703×10^{-2}	0.62050×10^{-2}	0.15000×10^{-2}
3.8800	-0.41143×10^{-2}	0.16203×10^{-2}	0.61700×10^{-2}	-0.21750×10^{-1}
3.9000	-0.40796×10^{-2}	0.18410×10^{-2}	0.51550×10^{-2}	-0.10250×10^{-1}
3.9200	-0.40408×10^{-2}	0.20349×10^{-2}	0.42800×10^{-2}	-0.12500×10^{-2}
3.9400	-0.39984×10^{-2}	0.22046×10^{-2}	0.39300×10^{-2}	-0.80000×10^{-2}
3.9600	-0.39528×10^{-2}	0.23522×10^{-2}	0.37950×10^{-2}	-0.20250×10^{-1}
3.9800	-0.39044×10^{-2}	0.24797×10^{-2}	0.00000	0.00000

REFERENCES

1. Iijima, S., *Nature*, 1991, **354,** 56.
2. For recent reviews see Ebbesen, T .W., *Physics Today*, 26 (June, 1996) and *Chem. Eng. Prog.*, 17 (March, 1997).
3. Iijima, S. and Ichlhashi, T., *Nature*, 1993, **363,** 603.
4. Bethune, D. S., Klang, C. H., De Vries, M. S., Gorman, G., Savoy, R., Vazquez, J. and Beyers, R., *Nature*, 1993, **363,** 605.
5. Ebbesen, T. W. and Ajayan, P. M., *Nature*, 1992, **358,** 220.
6. Mintmire, J. W., Dunlap, D. I. and White, C. T., *Phys. Rev. Lett.*, 1992, **68,** 631.
7. Hamada, N., Sawad, S. and Oshiyamu, A., *Phys. Rev. Lett.*, 1992, **68,** 1579.
8. Saito, R., Fujita, M., Dresselhaus, G. and Dresselhaus, M. S., *Phys. Rev. B*, 1992, **46,** 1804.
9. White, C. T., Robertson, D. H. and Mintmire, J. W., *Phys. Rev. B*, 1993, **47,** 5485.
10. Hamada, N., Sawada, S. and Oshiyama, A., *Phys. Rev. Lett.*, 1992, **68,** 1579.
11. Setlur, A. A., Lauerhaas, J. M. and Chang, R. P. H., *Appl. Phys. Lett.*, 1996, **69,** 345.
12. Thess, A., Lee, R. and Smalley, R. E., *Science*, 1996, **273,** 483.
13. Pederson, M. R. and Broughton, J. Q., *Phys. Rev. Lett.*, 1992, **69,** 2689.

14. Tersoff, J. and Ruoff, R. S., *Phys. Rev. Lett.*, 1994, **73,** 676.
15. Overney, G., Zhong, W. and Tomanek, D., *Z. Phys. D*, 1993, **27,** 93.
16. Robertson, D. H., Brenner, D. W. and Mintmire, J. W., *Phys. Rev. B*, 1992, **45,** 12592.
17. Molina, J. M., Savinsky, S. S. and Khokhriakov, N. V., *J. Chem. Phys.*, 1996, **104,** 4652.
18. Yakobson, B. I., Brabec, C. J. and Bernholc, J., *Phys. Rev. Lett.*, 1996, **76,** 2511.
19. Ajayan, P. M., Stephan, O., Colliex, C. and Trauth, D., *Science*, 1994, **265,** 1212.
20. Treacy, M. M. J., Ebbesen, T. W. and Gibson, J. M., *Nature*, 1996, **381,** 678.
21. Thess, A., Lee, R., Nikolaev, P., Dai, H., Petit, P., Robert, J., Xu, C., Lee, Y. H., Kim, S. G., Rinzler, A. G., Colbert, D. T., Scuseria, G. E., Tomanek, D., Fischer, J. E. and Smalley, R. E., *Science*, 1996, **273,** 483.
22. Ref. [16] found the difference in the numerical second derivative of energy with respect to strain along the tubule axis between tubules with diameters of 0.4 and 1.8 nm to be about 2 eV atom^{-1}.
23. Cornwell, C. F. and Wille, L. T., *Solid State Commun.*, 1997, **101,** 555.
24. Sinnott, S. B., White, C. T. and Brenner, D. W., in *Science and Technology of Fullerene Materials*, ed. P. Bernier, D. S. Bethune, L. Y. Chiang, T. W. Ebbesen, R. M. Metzger and J. W. Mintmire, MRS Symposia Proceedings No. 359. Materials Research Society, Pittsburgh, PA, 1995, pp. 241–246.
25. Askeland, D. R., *The Science and Engineering of Materials*, 3rd edn. PWS Publishing, Boston, 1994.
26. Chernozatonskii, L. A., Kosakovskaja, Z. Ja., Fedorov, E. A. and Panov, V. I., *Phys. Lett. A*, 1995, **197,** 40.
27. When the tubules in ref. [26] were removed from the silicon surface, it was discovered that they had capped ends. This suggests that the tubule film is bonded to the surface by van der Waals chemical bonds, although no mention of the strength of the tubule–surface bond is mentioned in ref. [26].
28. Henein, G. E. and Hillard, J. E., *J. Appl. Phys.*, 1983, **54,** 728.
29. Brenner, D. W., Sinnott, S. B., Shenderova, O. A. and Harrison, J. A., unpublished; Brenner, D. W., *Phys. Rev. B*, 1990, **42,** 9458.
30. Field, J. E., *The Properties of Diamond.* Academic Press, London, 1979.
31. See, for example, *Hornady Handbook*, 3rd edn. Hornady Manufacturing Company, Inc., Grand Island, 1982.
32. Vitek, V. and Egami, T., *Phys. Status Soldi B*, 1987, **144,** 145.
33. Sines, G., *Elasticity and Strength.* Allyn and Bacon, Inc., Boston, 1969.
34. Yu, J., Kalia, R. K. and Vashishta, P., *J. Chem. Phys.*, 1995, **103,** 6697.
35. Taylor, R. S. and Garrison, B. J., *J. Am. Chem. Soc.*, 1994, **116,** 4465.
36. Harrison, J. A., Brenner, D. W., White, C. T. and Colton, R. J., *Thin Solid Films*, 1991, **206,** 213.
37. Harrison, J. A., White, C. T., Colton, R. J. and Brenner, D. W., *Surf. Sci.*, 1992, **271,** 57.
38. Brenner, D. W. and Harrison, J. A., *Ceramic Bulletin*, 1992, **71,** 1821;Peploski, J., Thompson, D. L. and Raff, L. M., *J. Phys. Chem.*, 1992, **96,** 8539;Chang, X. Y., Thompson, D. L. and Raff, L. M., *J. Chem. Phys.*, 1993, **100,** 1765;Garrison, B. L., Dawnkaski, E. J., Srivastava, D. and Brenner, D. W., *Science*, 1992, **271,** 57;Alfonso, D. R. and Ulloa, S. E., *Phys. Rev. B*, 1993, **48,** 12235.
39. Harrison, J. A., White, C. T., Colton, R. J. and Brenner, D. W., *MRS Bull.*, 1993, **18,** 50.
40. Sinnott, S. B., Colton, R. J., White, C. T. and Brenner, D. W., *Surf. Sci.*, 1994, **316,** L1055.
41. Robertson, D. H., Brenner, D. W. and White, C. T., *J. Phys. Chem.*, 1992, **96,** 6133.
42. Williams, E. R., Jones, G. C., , JrFang, L., Zare, R. N., Garrison, B. J. and Brenner, D. W., *J. Am. Chem. Soc.*, 1992, **114,** 3207.
43. Moller, M. A., Tildsley, D. J., Kim, K. S. and Quirke, N., *J. Chem. Phys.*, 1991, **94,** 8390.